Automatika

Journal for Control, Measurement, Electronics, Computing and Communications

ISSN: (Print) (Online) Journal homepage: https://www.tandfonline.com/loi/taut20

Controlling the Speed of renewable-sourced DC drives with a series compensated DC to DC converter and sliding mode controller

K. Gurumoorthy & Sujatha Balaraman

To cite this article: K. Gurumoorthy & Sujatha Balaraman (2023) Controlling the Speed of renewable-sourced DC drives with a series compensated DC to DC converter and sliding mode controller, Automatika, 64:1, 114-126, DOI: 10.1080/00051144.2022.2118099

To link to this article: https://doi.org/10.1080/00051144.2022.2118099

Published online: 14 Sep 2022.

AUTOMATIKA
2023, VOL. 64, NO. 1, 114–126
https://doi.org/10.1080/00051144.2022.2118099

REGULAR PAPER

OPEN ACCESS Check for updates

Controlling the Speed of renewable-sourced DC drives with a series compensated DC to DC converter and sliding mode controller

K. Gurumoorthy[a] and Sujatha Balaraman[b]

[a]Department of EEE, Amrita College of Engineering and Technology, Nagerkoil, Tamil Nadu, India; [b]Department of EEE, Government College of Technology, Coimbatore, Tamil Nadu, India

ABSTRACT

A solar-powered drive for the separately excited DC (SEDC) motor drive system has been proposed and validated. The proposed system uses a set of two cascaded series compensated buck boost converters (SCBBCs) and a push pull DC to DC converter. The maximum power point tracking (MPPT) for the solar PV energy harvesting system is based on a sliding mode controller (SMC) and the SCBBC next to the solar PV source is used for this purpose. The armature winding of the SEDC motor receives the required isolated DC voltage from a push pull converter that is powered from a common DC link that carries a battery. The field winding of the SEDC motor is fed by the second SCBBC. The speed of the SEDC motor is regulated by a separate sliding mode controller implemented in the second SCBBC. A detailed state space analysis of the SCBBC and related mathematical modelling of the complete system are presented. The simulations were carried out in the MATLAB SIMULINK environment, and an experimental prototype was developed utilizing a 200 W 110 V SEDC motor.

ARTICLE HISTORY
Received 10 October 2020
Accepted 23 August 2022

KEYWORDS
Solar photo voltaic systems; series compensated buck boost converter; sliding mode controller; average state space modelling; speed regulation of DC motors

1. Introduction

Industrial drives benefit greatly from DC motors. They have practical control capabilities that allow the user to manage the speed and torque independently. With independent windings for the armature and field systems, the SEDC motor allows for easy and decoupled speed and torque control. The motor's speed can be adjusted while keeping a steady torque, and the torque can be adjusted for a constant speed.

Fixed torque variable speed mode (also known as variable power mode) and variable torque variable speed mode (also known as fixed power output mode) are the two operational modes. The amount of power delivered to the motor varies with speed and torque. It is possible to drive with constant power delivered to the motor while speed and torque are adjusted in a linked way using the SEDC motor.

The scope of this study is limited to the operation of a SEDC motor with speed control in variable power, constant speed and variable torque modes. A variety of controllers, such as the PI, PID, Fuzzy Controller, ANN and ANFIS-based controllers, are extensively used to regulate the speed of the SEDC motor.

Also, conventional power electronic converters such as the buck, buck boost and boost converters have all been extensively employed as DC motor drives. While the buck converter is designed to reduce the available input voltage, the buck boost converter may both step up and step down the supplied input voltage while the polarity of the output voltage is flipped in relation to the polarity of the input voltage. The boost converter can only increase the input voltage and cannot be reduced to a value less than the input voltage.

A design developed from the buck boost converter is the series compensated buck boost converter (SCBBC). The SCBBC's voltage gain is equivalent to that of a standard boost converter. It can't create a lower output voltage than the source voltage. The benefit of the SCBBC is that the converter only has to transport a portion of the total power given to the load; the remaining power, in this case, a SEDC motor, goes directly to the load. The SCBBC has minimal switching losses and requires a smaller capacity than the actual power being sent from the supply to the load.

A variety of contributions for the management of the SEDC motor has been provided in the literature. For the control of SEDC motors, PI and PID controllers have been frequently utilized [1]. Many researchers have suggested for double loop PI controllers with armature current limiting features [2]. For the regulation of the SEDC's speed, there have been several different types of PI and PID controllers. Many scholars have also developed modern intelligent controllers, such as fuzzy controllers, ANN-based controllers and ANFIS-based controllers [3–5].

CONTACT K. Gurumoorthy kgurumoorthy0401@gmail.com, gurumoorthy.k@kit.edu.in Department of EEE, Amrita College of Engineering and Technology, Nagerkoil, Tamil Nadu, India

With the introduction of the digital computer and the search algorithms such as the Genetic Algorithm (GA) [6], Particle Swarm Optimization (PSO) algorithm, and others, the tuning of PI or PID controllers is now a sophisticated processes [7–9].

The sliding mode controller (SMC) is a nonlinear control approach that is particularly suited to variable structure systems, such as discretely switched power electronic converters [10]. The SMC uses a nonlinear control method that works well with nonlinear power electronic converters. In its most basic version, the SMC-based nonlinear control system for nonlinear power electronic converters does not necessitate the use of common local linearization techniques and small signal analysis, etc. [11]. In the harvesting of solar photovoltaic electricity, the sliding mode controller can also be employed as a maximum power point tracking controller in conjunction with a power electronic converter [12].

Locally generated renewable energy sources are unavoidable in distant regions when access to the national grid is unavailable. DC motors offer a wide range of applications in both industrial and large-scale construction projects. Solar photovoltaic sources could be used to power DC motors at remote areas [13]. Maximum power point techniques, as well as speed management techniques, are required for solar photovoltaic sources utilized in industrial drives [14].

Power electronic converters, especially DC to DC converters, are capable of extracting the maximum amount of power from a solar PV system [15] and are also appropriate for controlling the speed of SEDC motors [16–18]. Solar power has been used for driving a brushless DC motor (BLDC) for a water pumping system, by the authors in Ref. [19]. In Ref. [20], a novel fuzzy cognitive network-based controller for the PV-fed DC motor has been presented. The authors in Ref. [21] have developed a peak current detection method for the speed regulation of a sensor less BLDC motor-driven irrigation pump. An improved fuzzy logic controller for the speed regulation of a permanent magnet BLDC motor has been presented in Ref. [22]. Solar-powered water pumping schemes have also used permanent magnet synchronous motors as well as demonstrated by the authors in Ref. [23].

The PI controllers have been traditionally used for the speed regulation of the DC motors and in the research contribution of the authors in Ref. [9] a novel tuning technique for the PI controller by the particle swarm optimization (PSO) method has been presented. The authors in Ref. [24] have developed a power-efficient control scheme for powering up a solar-powered DC motor-based pump using a three-level DC to DC converter.

Despite the proliferation of the DC to DC converter topologies and the MPPT as well as control schemes, there had not been a single study made on the SCBBC. In this work, the SCBBC is used as an interface between the solar PV source and the battery as well it is used as a boost converter to drive the SEDC motor. It has been established that the SCBBC is amenable for implementing MPPT for solar PV system while it is also useful as a speed regulator for the SEDC motor.

In this work, a set of two cascaded DC to DC converters of the SCBBCs are used for solar power harvest as well as speed regulation of the SEDC motor. In order to provide power backup, a battery is connected in between the two SCBBC units so that the solar power harvested is routed to the battery and the battery gets charged and the SCBBC next to the battery drives the DC motor and proper speed regulation arrangements are provided.

The novelty of the work is that the proposed system demonstrates the usage of the SCBBC for voltage step up and MPPT. Similarly, for the purpose of voltage step-up action and for speed regulation another SCBBC is used. The SCBBC is a buck boost converter with the advantage that only a portion of the power being transacted has to pass through the converter and the remaining part of the power flows directly to the load. This leads to reduced power loss as well the power handling capacity of the power electronic converter is much less than the power that is actually transacted.

The rest of the paper is arranged as follows. Next to this introduction presented as Section 1, the block schematic of the proposed system is explained in Section 2. The details of the SCBBC are discussed in Section 3. The applicability of the sliding mode controller (SMC) for MMPT is discussed in Section 4. The details of the push pull DC to DC converter which provides an isolated power supply for the armature winding is discussed in Section 5.

2. The block schematic of the proposed system

The suggested SEDC motor drive's block diagram is shown in Figure 1. The solar PV module, SCBBC1 at the front end, the battery, SCBBC2 that powers the SEDC's armature, and a push pull DC to DC boost converter that drives the field winding are the primary subsystems. The SCBBC1 receives and transmits solar PV electricity to the battery. Maximum power point tracking is handled by the SCBBC1. The SCBBC2 boosts the battery's nominal 24 V and feeds power to the SEDC motor's armature circuit. The field winding provided by the Push Pull Converter is used to excite the SEDC. The push pull converter has a high voltage gain and offers the necessary isolation between the armature and field windings of the SEDC motor. The system has a 250 W nominal power rating. Table 1 lists the parameters of the converter subsystems.

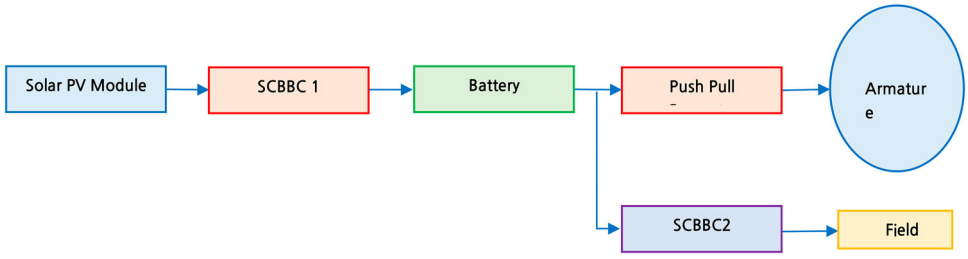

Figure 1. The block schematic of the proposed SEDC motor drive.

Table 1. Specifications of subsystems in simulation.

Solar PV module	250 W (125 W *2)
Vpmax	17.19 V
Ipmax	7.28 A
Voc	21.58 V
Isc	7.89 A
SCBBC 1	
Power electronic switches	MOSFET 1 Diode 1
Capacitor	2200 MFD
Inductor	1 mH
Battery	24 V 60 AH
SCBBC2	
Power electronic switches	MOSFET 1 Diode 1
Inductor	1 mH
Capacitor	2200 MFD
Push pull converter	
Transformer	24 0 24/220 V 50 Hz 250 VA
Rectifier	Diode Bridge Rectifier
Primary side switches S1 and S2	MOSFETs

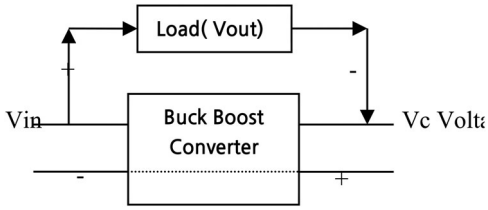

Figure 2. The scheme of the SCBBC.

3. The SCBBC and its modelling

The SCBBC's scheme is depicted in Figure 2. The structure is similar to that of a buck boost converter in general. The load is linked across the load side capacitor in a basic buck boost converter.

The supply and the regular load side capacitor share a same connection. The load is connected between the source's positive terminal and the load side capacitor's negative terminal. The voltage across the output side capacitor and the source voltage act in series and are additive.

Figure 3 depicts the topology of the SCBBC. $(d)/(1-d)$ is the voltage gain of a standard Buck boost converter, where d is the duty cycle. When Vin is 24 V and d is 0.8, the output voltage is $24 * 0.8/0.2 = 96$ V. Vc denotes the voltage that appears across the output capacitor. The overall output voltage of the SCBBC is the sum of the input voltage Vin and the voltage across

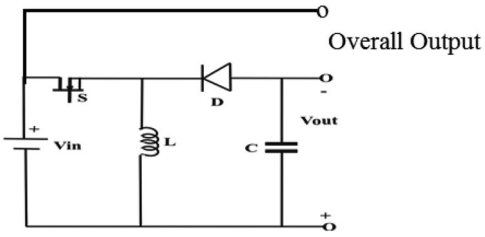

Figure 3. The topology of the SCBBC.

the output capacitor Vc.

$$\text{Vout} = \text{Vin} + \text{Vc} = 24 + 96 = 120\text{V}.$$

By applying simple mathematical manipulations,

$$\text{Vout} = \text{Vin} + \text{Vc} \tag{1}$$

Where

$$\text{Vc} = \text{Vin} * \left(\frac{d}{1-d}\right) \tag{2}$$

Therefore

$$\text{Vout} = \text{Vin} + \left(\text{Vin} * \left(\frac{d}{1-d}\right)\right) \tag{3}$$

$$\text{Vout} = \text{Vin} + (\text{Vin} * d)/(1-d) \tag{4}$$

$$= \text{Vin}(1 + d(1-d)) = \text{Vin}/(1-d) \tag{5}$$

With a duty cycle of 0.8, a buck boost converter has a voltage gain of 4 and the SCBBC has a voltage gain of 5. If Vin = 24 V, the SCBBC's output voltage is 120 V, according to the example. The load current becomes 1 A and the power provided to the load is 120 W if the load resistor is 120 Ohms. A portion of this power, 24 W, is delivered directly to the load from the source. The SCBBC must handle the remaining 96 W. The state equations of the SCBBC can be developed using fundamental principles and its implementation in MATLAB SIMULINK is shown in Figure 4.

4. SMC for MPPT at the SCBBC

Maximum power point tracking (MPPT) is a technique for extracting the most power from a solar PV panel for a given sun irradiation and temperature. When the weather changes, the internal characteristics of the SPV modules change, and the load should be adjusted correspondingly to ensure that the greatest amount of power

is delivered from the source to the load. There is a power control switch S in the case of SCBBC. The SPV drives a large current through the inductor when switch S is closed. The SPV drives a current through the load and the capacitor C in series with the load when the switch is opened.

By controlling the durations of the On and Off periods in each switching cycle, in an automated manner, the power harvested from the solar PV panel may be maximized. With reference to Figure 5, there are two curves. The first curve relates the voltage across the SPV panel and the SPV output current. The second curve relates the voltage across the PV panel and the power being harvested. There exists a unique operating point with Vpmax the terminal voltage and Ipmax the solar PV current that delivers maximum power output. The sliding mode controller keeps the optimal terminal voltage across the SPV panel for any given solar insolation so that the maximum power is harvested.

5. Push pull DC to DC converter

A pair of power electronic switches and a step-up transformer with a Centre taped low voltage primary winding are used in a push pull DC to DC converter. The benefit of a push pull converter is that it produces a high voltage gain, which is controlled by the transformer's turn ratio. In addition, the push pull DC to DC converter isolates the source and load sides. Separate power sources are required for the armature and field windings in the SEDC drive. The SCBBC provides the desired excitation voltage to the field winding, and the field current is regulated by the PWM implemented in the SCBBC.

The armature winding of the proposed SEDC drive is provided by a push pull DC to DC converter that delivers a DC voltage of 110 V DC nominally. The battery powers the push pull DC to DC converter. The field winding of the SEDC, on the other hand, is powered by the battery in the common DC link and stepped up by the SCBBC.

Thus, the duty cycle of the SCBBC may be altered to regulate the voltage delivered to the field winding, and the duty cycle of the push pull DC to DC converter can be changed to modify the armature current. Figure 6 depicts the structure of a push pull converter.

6. Speed regulation of the SEDC motor using the push pull converter with SMC

For a constant load torque, the speed of the SEDC motor can be modified by altering the duty cycle of the PPC, which changes the voltage provided to the SEDC. A small shift in duty cycle causes the voltage delivered to the armature of the SEDC to increase, and hence the armature current, with a given present speed and thus for a given back EMF. When the field current is kept constant, an increase in the armature current increases the electromagnetic torque produced, and the speed increases until it reaches a steady-state speed. The electromagnetic torque produced at the new steady state is adequate to drive the load at the maximum speed.

Similarly, the duty cycle of the PPC can be adjusted to lower the voltage delivered across the armature of the SEDC, lowering the armature current and, as a result, the electromagnetic torque produced, lowering the speed. The speed is controlled by controlling the armature current while the field current is kept constant. This is known as a variable speed variable power method. The motor's mechanical load torque is the same in this control mode.

A closed-loop controller is required to regulate the speed of the SEDC motor. The DC motor's speed is the controllable parameter, whereas the duty cycle is the controlled parameter. The SEDC motor's speed is determined by the voltage between the armature terminals, while the field current and load torque on the machine shaft are kept constant.

When the mechanical load torque on the shaft is increased from one value to another, the motor's speed decreases, the back EMF decreases, and the motor draws more current from the supply. As a result of the higher armature current, higher torque is generated, and the speed is returned to its previous level. The motor is now drawing more power.

7. Sliding mode controller-based speed regulation

The SMC determines the SEDC's real speed. The user is in charge of the set point speed. Error is defined as the difference between the set and actual speed. If the desired speed is higher than the actual speed, the error is positive. If the actual motor speed is higher than the set speed, the error is negative.

A constant duty cycle is used in the operation of the SMC, and a stream of pulses is constantly generated. A gating mechanism applies the stream of switching pulses to the gate of the PPC's power control switches S1 and S2. Only when the error is positive does the gating system allow switching pulses to the MOSFETs. When the error is negative, the gating system prevents switching pulses from reaching the power electronic switches.

The algorithm can be stated as

$$\text{If error} > 0 \text{ then gate} = 1;$$

$$\text{If error is} < 0 \text{ then gate} = 0;$$

Speed regulation is accomplished by employing this easy approach. The only need is that the duty cycle chosen be capable of pushing the controlled parameter from its starting value to its required value when the initial value is less than the specified value. The next

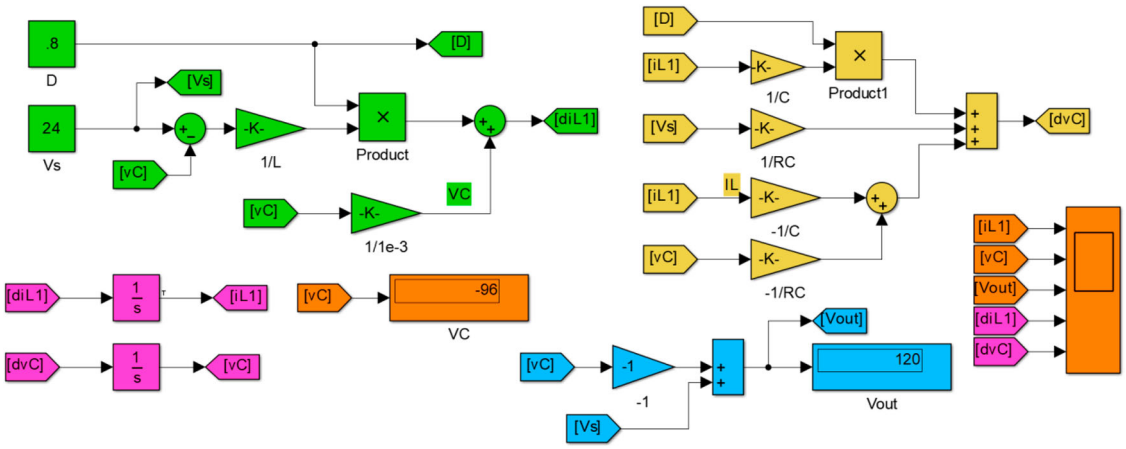

Figure 4. The MATLAB SIMULINK implementation of the state space model of the SCBBC.

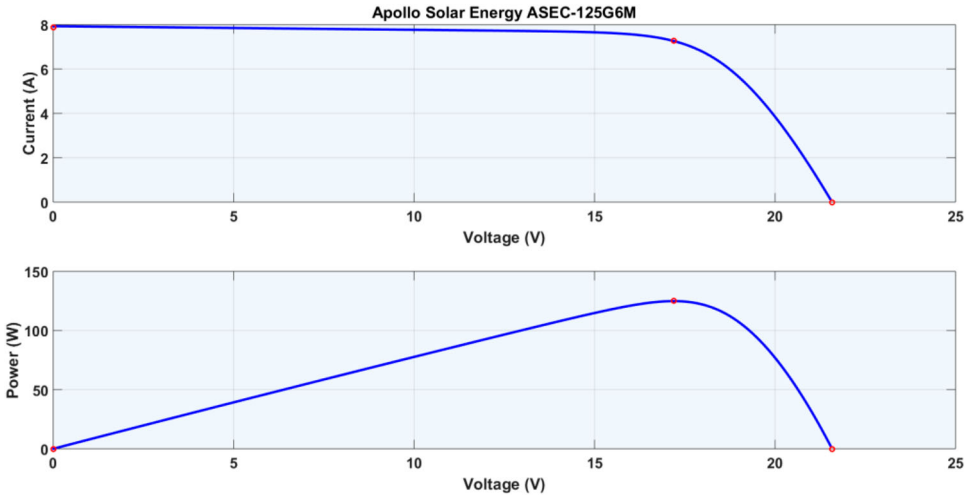

Figure 5. The V-I and V-P characteristics of one of the 10 parallel connected SPV panels.

sections describe the implementation plan of the sliding mode controller for regulating the speed of the SEDC motor.

8. Realization in MATLAB SIMULINK

Figure 7 shows the main page of the MATLAB SIMULINK realization of the proposed scheme. The subsystems are presented in Figures 8–10. In this work, the main source of electrical power is derived from the solar photo voltaic (SPV) panel. The harvested solar energy is stored in a battery. The MPPT is governed by a sliding mode controller. The sliding mode controller for MPPT is implemented in the SCBBC1 that is interfaced between the Solar PV source and the battery. The solar PV subsystem, the SCBBC 1 and the battery are shown in Figure 8. The solar PV subsystem and the SMC implementation are shown in Figures 9 and 10. The

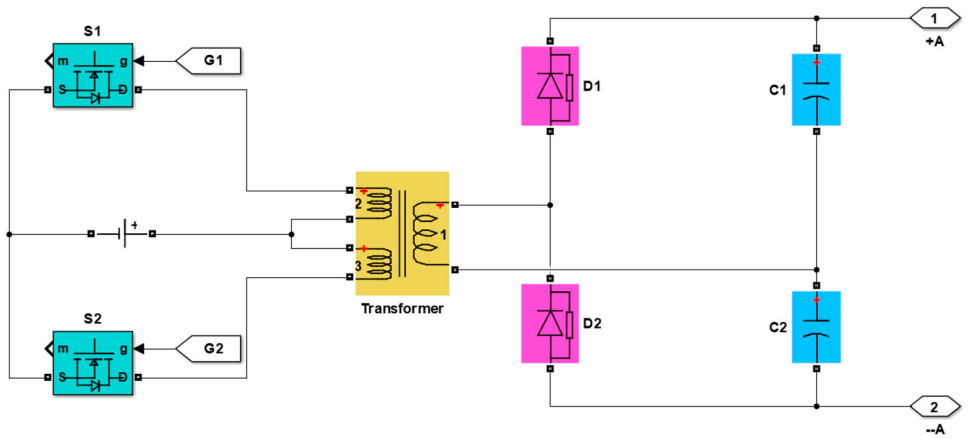

Figure 6. The topology of the push pull converter.

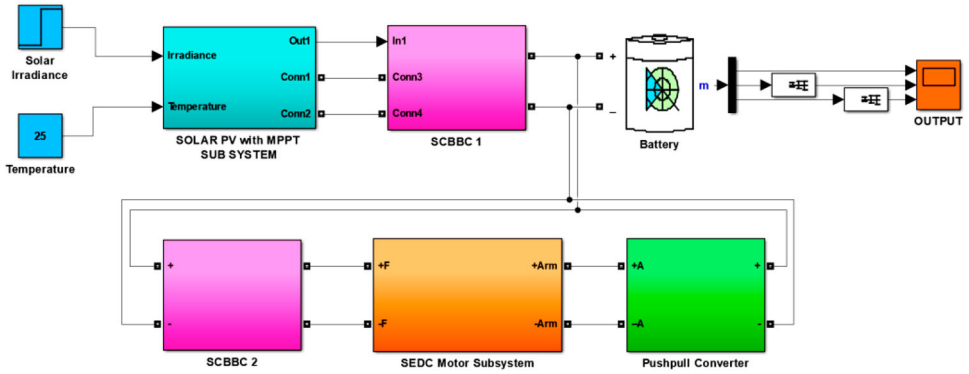

Figure 7. The MATLAB SIMULINK realization of the complete proposed system.

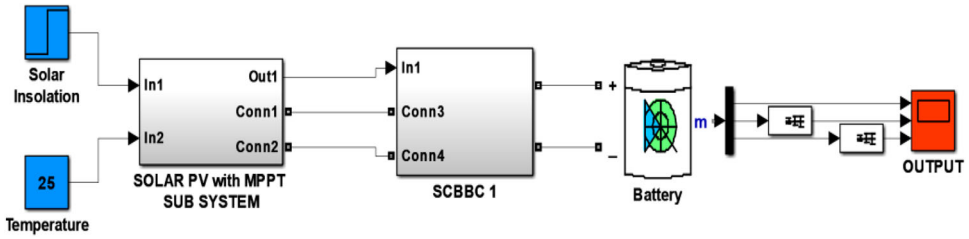

Figure 8. The battery charging subsystem using solar PV source.

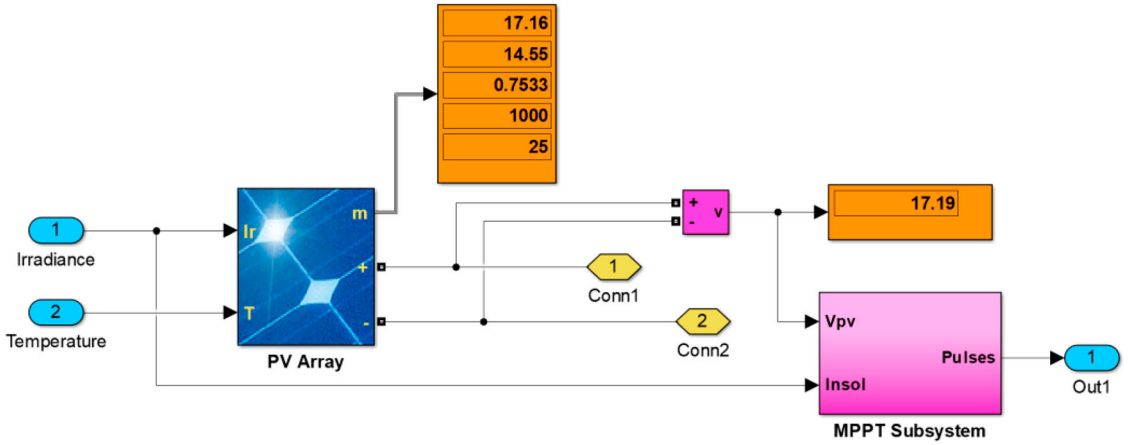

Figure 9. The Solar PV subsystem with the MPPT subsystem.

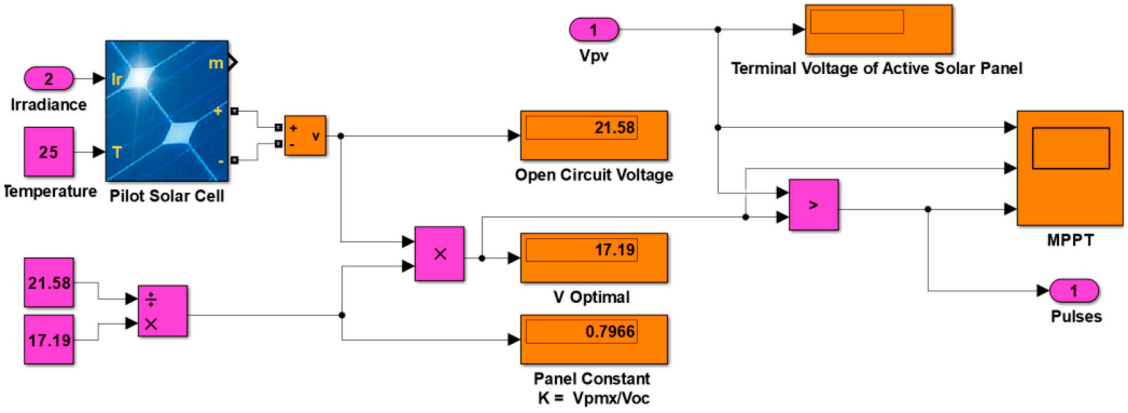

Figure 10. The realization of the sliding mode controller with the pilot SPV module.

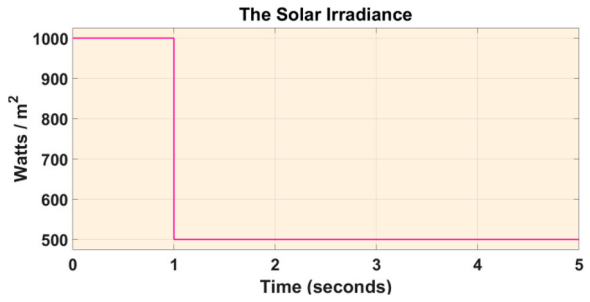

Figure 11. The solar irradiance with a step change occurring at time instant 1 s.

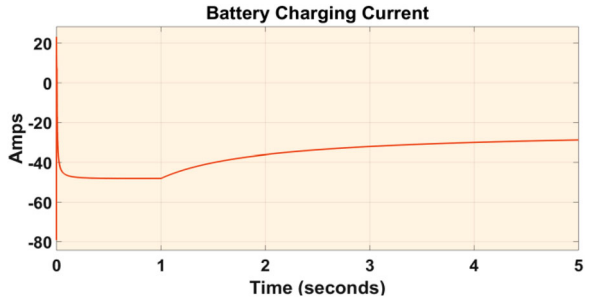

Figure 12. The battery charging current.

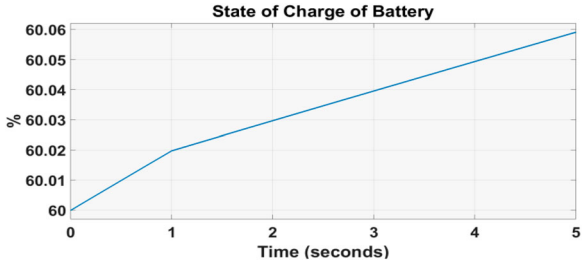

Figure 13. The changes in the rate of rise of SOC for different solar irradiances.

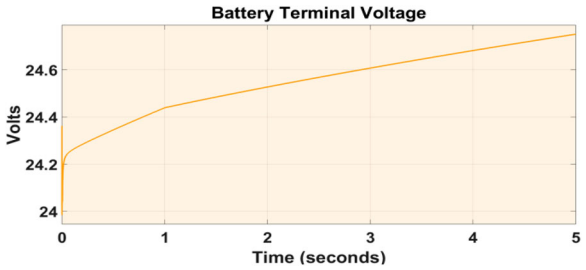

Figure 14. The different rates of rise of terminal voltage of the battery.

results of simulation of MPPT for the SPV implemented in the SCBBC1 are shown in Figures 11–14.

In Figure 11, there is a step change in irradiance from 1000 W/m^2 to 500 W/m^2 at time instant 1 s. Correspondingly, as shown in Figure 12, the battery charging current is initially around 48 A and after the solar irradiance comes down to 500 w/m^2 at time instant 1 s the charging current comes down to around 29 A. In accordance with the variations in the charging current, the rate of rise of the SOC of the battery also gets changed. The rate of rise of SOC is more between time interval 0

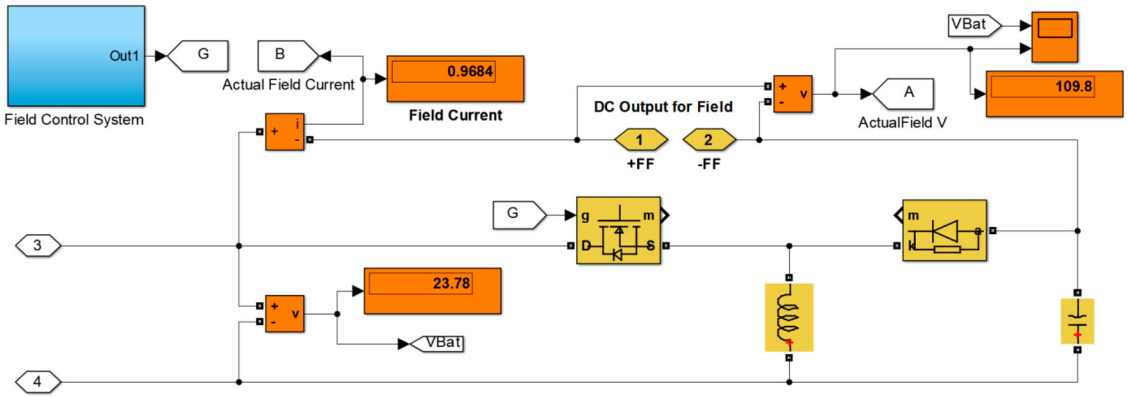

Figure 15. The SIMULINK realization of the Field circuit control using the SCBBC.

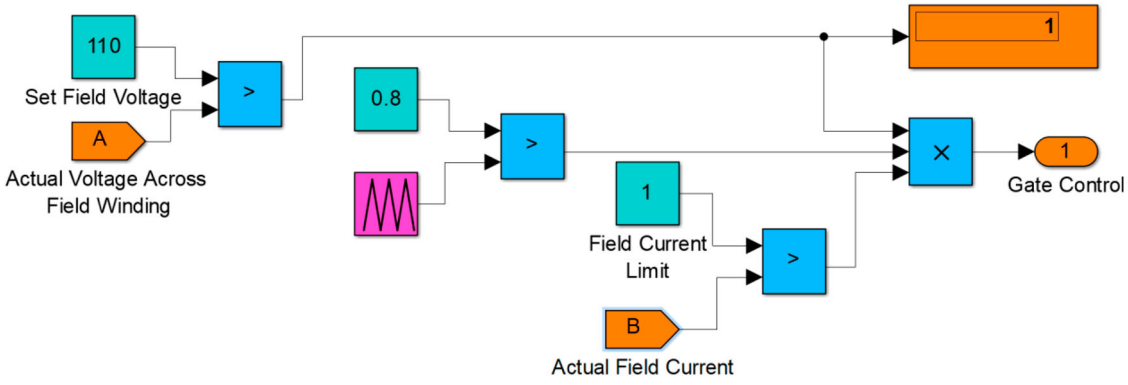

Figure 16. The control circuit used for the management of the field winding excitation.

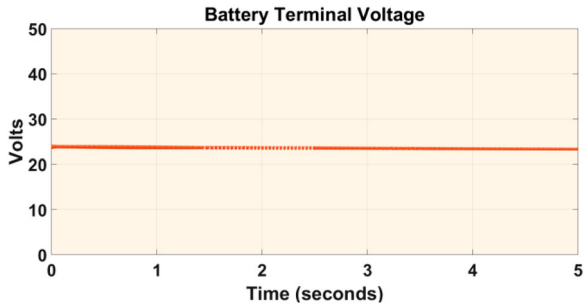

Figure 17. The battery terminal voltage.

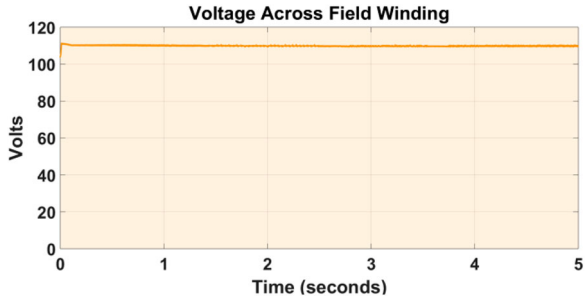

Figure 18. The regulated 110 V voltage impressed across the field winding.

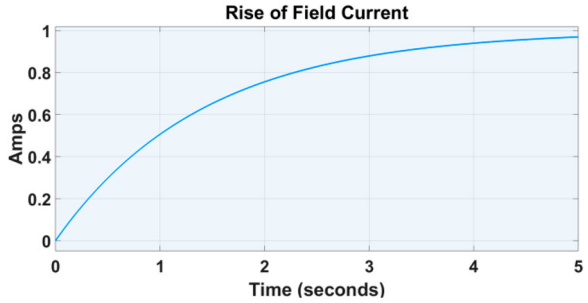

Figure 19. The rise of the field current from 0 A towards the maximum allowable 1 A limit.

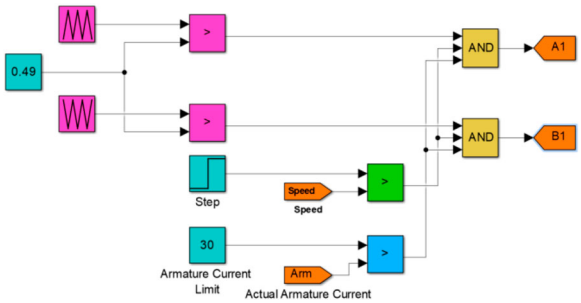

Figure 21. The speed control scheme implemented on the push pull converter.

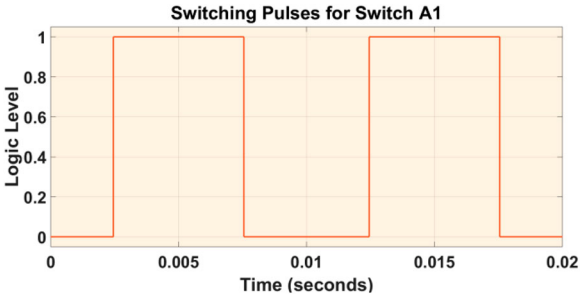

Figure 22. The switching pulse for Switch A1 of PPC.

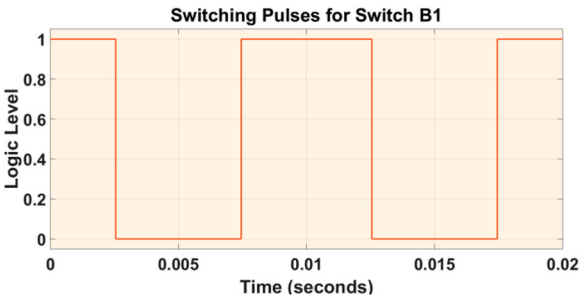

Figure 23. The switching pulse for Switch B1 of PPC.

and 1 s while the rate of rise of SOC is lowered beyond the 1 s instant as shown in Figure 13. The corresponding variations in the terminal voltage of the battery are shown in Figure 14.

Figure 15 shows the implementation of the SCBBC used for the control of the field circuit. The input power is drawn from the battery and the required voltage for the field winding is derived across the output terminals of the SCBBC. The control subsystem for the field circuit is represented as a block in Figure 15 and the contents of this block are given in Figure 16.

Figure 16 shows the control circuit used for the regulation of the field winding voltage and the field current

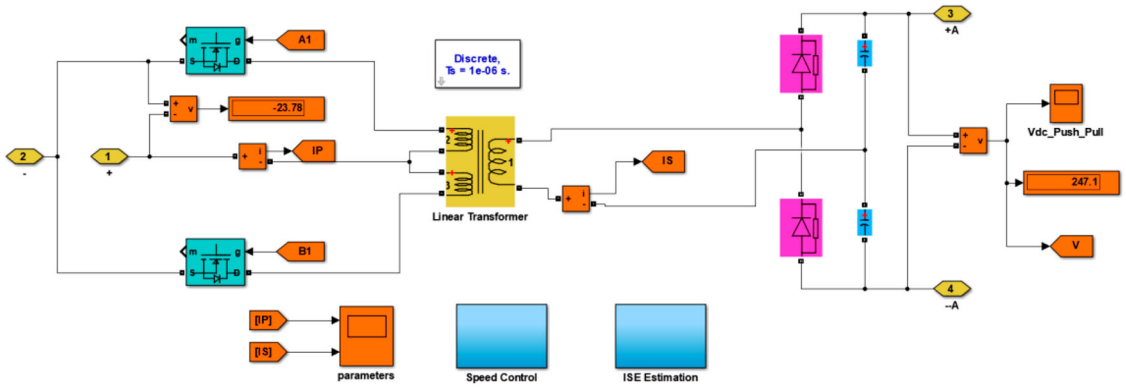

Figure 20. The push pull converter that feeds the armature of the SEDC.

limitations. The set voltage to be maintained across the field winding is 110 V and there is a current limiting of 1 A. This subsystem produces a train of square pulses at a frequency of 5 kHz with a fixed duty cycle of 80%. However, whether to apply this train of square pulses to the MOSFET in the SCBBC or not is constrained by the set voltage and the current limiter. Switching pulses are provided to the gate of the SCBBC MOSFET whenever the actual voltage across the field winding is less than 110 V and the field current is less than 1 A. The battery voltage, the voltage across the field winding and the field current waveform are shown in Figures 17–19.

Figure 20 shows the SIMULINK realization of the push pull converter (PPC) that feeds power to the armature circuit of the SEDC. The armature side control scheme is shown in Figure 21.

Figures 22 and 23 show the complementary switching pulses applied to the two switches of the PPC. With reference to Figure 21, the duty cycle is 0.49. The switching pulses to the two switches A1 and B1 are derived using the sliding mode control as shown in Figure 21. The set point speed and the actual speed are compared and the control bit which is 0 or 1 is generated. If the actual speed is less than the set speed, the control bit is 1 and 0 if the actual speed has crossed the set speed. Similarly, there is a current limit modules. When the armature current is less than 30 A the switching pulses are routed to the gates of the MOSFETs. Whenever the load current becomes more than 30 A the switching pulses are blocked from reaching the MOSFETs.

Figure 24 is shown the actual motor subsystem with a free wheel diode so as to maintain continuous current through the armature. However, this diode is not useful as the DC source for the armature circuit is already rectified and filtered.

The experiment started with a speed command of 500 RPM and was increased to 1500 RPM at time instant 3.5 s. There is also a command for the load torque which is initially maintained at 0 Nm initially and at time instant 0.5 s it has been changed to 2 Nm and at time instant 2.5 s it has further been changed to 3 Nm. The speed and the load torque commands given

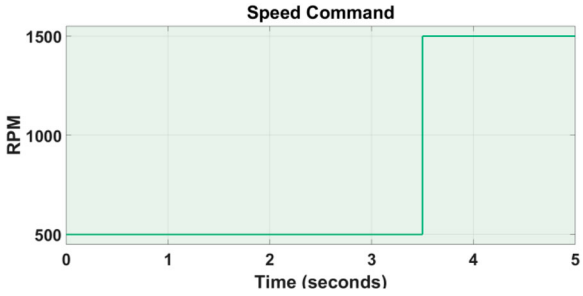

Figure 25. Step change in speed command.

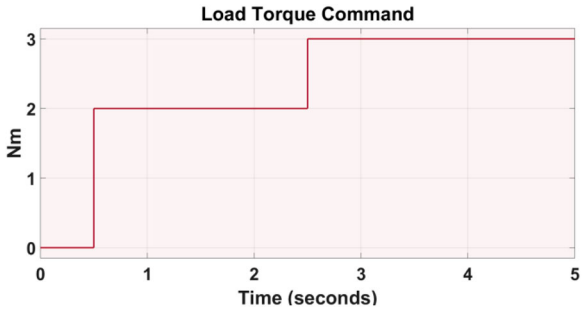

Figure 26. Step change in load torque command.

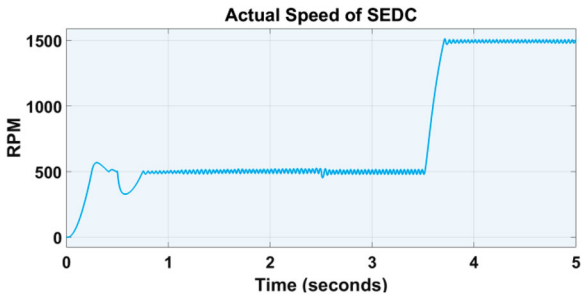

Figure 27. The speed response of the SEDC against variations in commands.

are shown in Figures 25 and 26, respectively. Figure 27 illustrates the SEDC's response in terms of speed.

With the initial load torque being 0 Nm, the motor picks up speed and rises towards the set value of 500 RPM. The speed settles down at 500 RPM level after an overshoot. The overshoot is high because of the lack of any load torque. Even as the motor starts

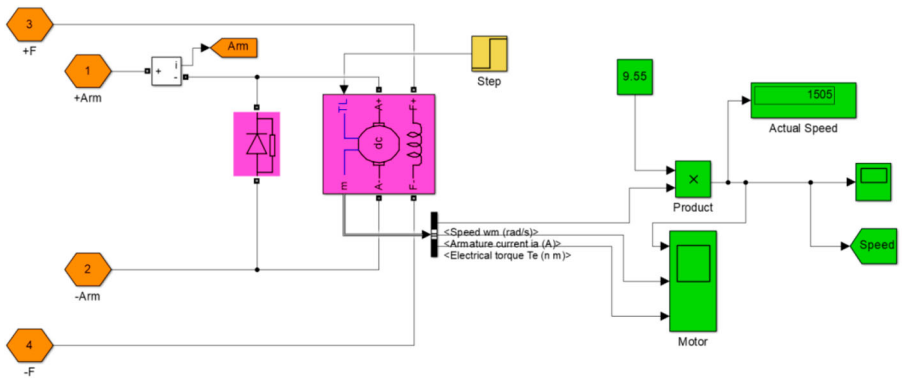

Figure 24. The armature circuit with a freewheel diode across the armature.

maintaining a speed of 500 RPM, at time instant 0.5 s a load torque of 2 Nm is applied and the speed suddenly drops. However, the closed-loop control scheme takes up the speed back to the 500 RPM level within a period of 0.25 s and the motor speed is regulated at 500 RPM until time instant 2.5 s. At time instant 2.5 s, a further increase of load torque from 2 Nm to 3 Nm is applied. The speed does not fall now. A very small disturbance to the speed is exhibited. The speed falls by around 30 RPM and picks up within a period of less than 0.1 s and continues at the speed of 500 RPM. At time instant 3.5 s, a change in the speed command from 500 RPM to 1500 RPM is applied and the motor speed rises up to the 1500 RPM level. There is no overshoot exhibited. It is the sliding mode controller that drives the speed from 500 RPM to 1500 RPM and maintains at 1500 RPM without any overshoot during the transient period.

When the speed command is changed from 500 RPM to 1500 RPM as shown in Figure 25, the performance of the sliding mode controller, in the regulation of speed of the DC motor, has been compared against the performance of the PI controller. By way of simulations in the MATLAB SIMULINK environment, it has been observed that the steady-state error, the integral square error, the peak overshoot and the transient period are all improved in the sliding mode controllers as compared to the PI controller as shown in the Table 2.

The loss analysis is an important aspect of the power electronic converter and the proposed system was also considered in this perspective of loss analysis and the estimation of power conversion efficiency. As for the topology, there are two sections. In the front end is a SCBBC and this unit is used for harvesting power from the solar PV source. If the inductor and the capacitor are considered to be ideal the only component that incurs possible loss is the power electronic switch. The power harvested from the solar panel and the power delivered to the battery may be considered for the estimation of the overall efficiency of this system. It has been observed that when the solar irradiance was kept at 1000 W/m^2 the terminal voltage and the output current of the SPV module were observed to be

$$(2 * 17.16)\ \text{V and}\ (5 * 14.85)\ \text{A giving a power} = 2548\ \text{W}.$$

The power delivered to the battery is 48 A $*$ 24.3 V $=$ 1166 W.

The remaining power is delivered to the motor. The power received by the motor can be calculated by the current drawn by the motor and the terminal voltage and it is

$$247\ \text{V} * 4.34\ \text{Amperes} = 1050\ \text{W}.$$

And the overall efficiency is (output power/ input power) $*$ 100 $=$ 87%.

Table 3. Loss analysis.

Component	Quantity of power
Power drawn from solar PV module	2548 W
Power delivered to battery for charging	1166 W
Power supplied to motor	1050 W
Overall efficiency	(1166 + 1050)/2548 = 87%
Total losses	312 W
Losses in field winding and transformer	120 W
Total losses in the semiconductors	212 W
Losses in SCBBC semiconductors	64 W
Losses in the push pull semiconductors	148 W

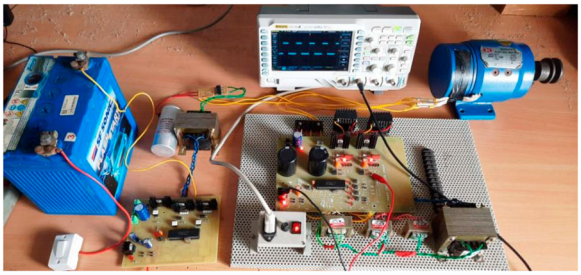

Figure 28. The layout of the subsystems in the prototype.

The total losses account to 332 W.

These losses occur in the three switches, three diodes and the AC link transformer. Considering the duty cycle and the measured average voltage and current through the switches and diodes the total losses in the semiconductors can be shown to be 212 W.

The losses occurring in the AC link transformer and the field winding account to the remaining 120 W.

Loss analysis in simulation under standard test conditions of Irradiance $=$ 1000 W/m^2 and temperature $=$ 25°C was carried out and presented in Table 3. The losses in the semiconductors have been estimated using the standard power equation $P = V * I$ after measuring the average voltage drop and current through the switches. However, the copper losses in the transformer windings and the field winding of the motor have been estimated using the equation $P = I^2 R$.

9. Experimental prototype

An experimental prototype has been created to validate the suggested concept. The prototype had a solar PV source, a SCBBC at the front end, a battery and another SCBBC to drive the DC motor's field winding and a push pull converter to drive the SEDC motor's armature winding. Table 4 lists the solar PV module and associated subsystem specifications. Figure 28 shows an image of the prototype.

The prototype uses the same circuit architecture as the simulation type. The battery unit receives energy from the solar PV unit. Two 12 V 35 AH batteries are connected in series to form the battery unit. Through the SCBBC1, the solar PV module charges the battery. The SEDC receives its armature power from the batteries through the push pull converter. The field excitation

Table 2. Time responses comparison with PI controller and SMC.

Controller	Steady-state error attained RPM	Peak over shoot attained RPM	Rise time in second	ISE
PI controller	12	48	0.48	2755
SMC	5	22	0.24	1455

Table 4. Specifications of Subsystems in proto type.

Subsystem	Specifications
Solar PV unit	
Voc	21.58 V
Isc	7.89 A
Vpmax	17.19 V
Ipmax	7.28 A
SCBBC 1	
Inductor	1 mH
Capacitor	2200 MFD
Power electronic switch	MOSFET IRF 540
Battery	12 V ∗ 2; 35 AH Each
SCBBC2	
Inductor	1 mH
Capacitor	2200 MFD
Power electronic switch	MOSFET IRF 840
Load	DC Motor 110 V 200 W

is supplied by the second SCBBC, and the power flow is as illustrated in the block diagram in Figure 1.

The specifications of various subsystems are shown in Table 4.

Separate PIC micro-controllers were used for the SCBBCs and the PPC. As for the MPPT of the SPV, the SMC scheme is used. Similarly, for the field winding control another SMC is used. These two SMCs use a common PIC micro-controller in which the input analogue parameters like the SPV terminal voltage and the filed winding voltage are measured. The two PWM schemes available in the PIC micro-controller are used for the SCBBC1 where the MPPT is implemented and the SCBBC2 which regulates the voltage across the field winding. The PPC which drives the armature circuit of the SEDC is controlled by a separate PIC micro-controller. The armature voltage is used as a measure of the speed of the SEDC and this voltage is attenuated to 0–5 scale and fed as feedback to the micro-control analogue channel A0. The set point speed is supplied to the micro-controller using a preset using which an analogue voltage of 0–5 V may be supplied.

The MOSFETs are driven using opto-couplers. The opto-coupler MCT2E acts as the interface between the PIC micro-controller and the gate of the MOSFET. The switching pulses applied to the MOSFETS, the typical output waveforms and the speed response in accordance with the command have been recorded and some of the waveforms are presented herein.

In the proposed SCBBC-based drive of the SEDC motor, the PIC micro-controller 16F877A contains the closed-loop control system and the PWM section. Figure 29 shows the PWM pulses derived from the micro-controller for a duty cycle of 40%.

With the closed-loop controller in action, the speed of the SEDC is the controlled parameter and the duty

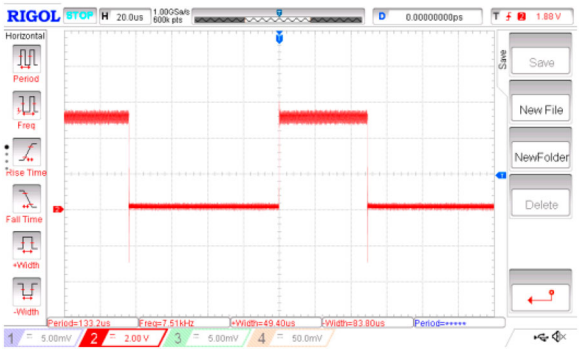

Figure 29. The switching pulses applied to the SCBBC.

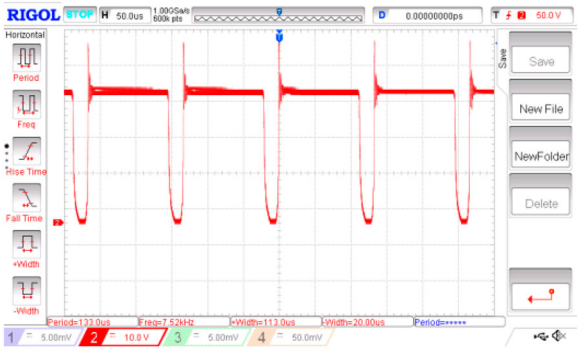

Figure 30. The voltage across the MOSFET of the SCBBC.

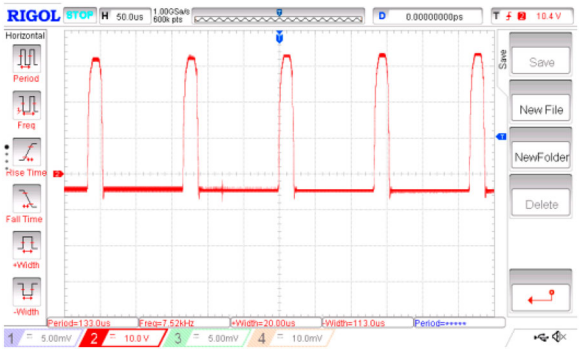

Figure 31. Voltage across the inductor of the SCBBC.

cycle used in the SCBBC is the manipulated parameter. Figure 30 shows the voltage across the MOSFET of the SCBBC when the duty cycle is nearly 19% for a speed of 400 RPM. The corresponding voltage across the inductor is shown in Figure 31.

The algorithm executed a speed command of 1400 RPM with a step change in speed command to 700 RPM. The SEDC's resulting speed response was observed and represented as a waveform in Figure 32. By measuring the motor current and armature resistance, the speed of the SEDC has been associated in an

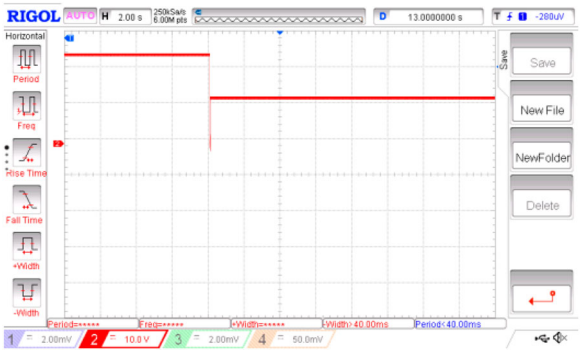

Figure 32. The speed of the SEDC motor with a speed command from 1400 RPM to 700 RPM.

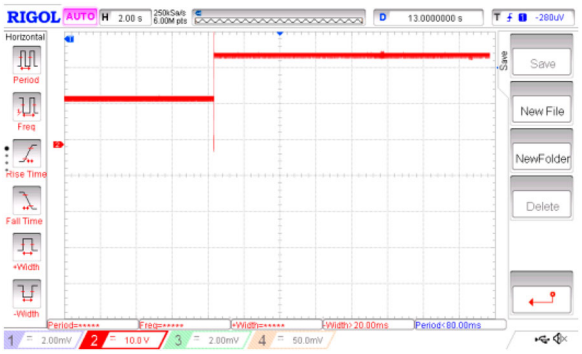

Figure 33. The speed of the SEDC motor with a speed command from 600 RPM to 1200 RPM.

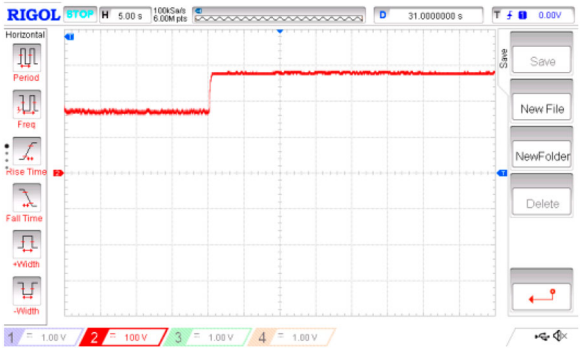

Figure 34. The transient of the armature current when the speed rises from 700 RPM to 1400 RPM.

indirect approach of determining the back EMF. Similarly, the response of the SEDC for a speed command from 600 RPM to 1200 RPM is shown in Figure 33.

While maintaining a fixed field current the armature current alone becomes the controllable parameter that modifies the torque and speed with a change in the solar irradiance. Since the load is considered constant, the change in solar irradiance causes a change in the applied voltage and it changes the armature current causing a change in the electromagnetic torque produced resulting in the change in the speed as shown in Figures 32 and 33. The armature current as a direct measure of the torque produced. The armature current for the transients has been recorded and has been presented herein in Figures 34 and 35.

Figure 35. The transient of the armature current when the speed falls from 1400 RPM to 700 RPM.

Table 5. Comparison of the super lift Luo converter with the proposed scheme.

Converter	Voltage gain	Transformer	ZVS	Efficiency	Switches
SL Luo	High	Not used	No	82%	1
Proposed system	Very High	Used	yes	87%	4

The proposed work uses a set of SCBBCs and a push pull converter. The push pull converter is advantageous because the power electronic switches are in the low voltage side with reduced voltage stress and losses incurred in the switches. The SCBBC offers more power conversion efficiency because it is only a part of the output power that flows through the converter and the remaining part flows direct to the load. The same application can be realized using boost converters. But the voltage gain of the boost converter is low in the stable low-duty cycle region. The proposed method gives a large overall voltage gain, achieved by the push pull converter, even for a small duty cycle. The voltage gain is determined by the turn's ratio of the push pull transformer. The proposed system works more stable and its power conversion efficiency can be compared with the generic converter and the super lift Luo converter as shown in Table 5. As compared to the efficiency of the super lift Luo converter which is around 82%, the proposed system offers an overall efficiency of 87%.

The speed control of the DC motor was carried out using the SMC. However in order to appreciate the performance of the SMC a PI controller was also programmed in the micro-controller and the results obtained separately in both cases were recorded and are presented herein. The comparison was carried out for a step speed command from 700 RPM to 1400 RPM.

The PI controller requires a precise mathematical modelling and it involves more mathematical overhead during design and programming. Also, since the PI controller involves mathematical calculations in every control cycle requires more memory and takes more time before decision making. Therefore, the SMC offers better dynamic performance and is more advantageous as shown in Table 6.

Table 6. Comparison of the performance of the PI and the SMC controllers.

Parameter considered	Sliding mode controller	PI controller
Steady-state error	17 RPM	24 RPM
Over shoot	26 RPM	48 RPM
Rise time	12 s	17 s
Integral square error	3420	4760
Mathematical over head in design	Less	More
Memory requirement	Less	More

10. Conclusion

A modern solar-powered SEDC motor driving method has been designed and tested in this paper. For connecting the SPV source to the battery, a SCBBC was employed. The field winding and armature winding were both powered by the battery. The voltage across the Field winding has been regulated using a SCBBC. The armature is being driven by a push pull converter. Three different control techniques have been implemented. In the first SCBBC, one SMC for the MPPT of the SPV was implemented. The voltage across the field winding has been controlled by the second SMC. The third SMC is employed to control the duty cycle of the PPC that powers up the armature circuit, allowing it to regulate the speed of the SEDC.

The proposed concept was validated by modelling in the MATLAB SIMULINK environment and an experimental prototype. According to the findings, the SCBBC is a better choice than a conventional boost converter, and the SMC is a superior choice for MPPT of solar PV because it just requires the voltage across the SPV panel for control systems. Furthermore, when compared to a PI controller, the SMC has less peak overshoot, steady-state error and ISE.

Disclosure statement

No potential conflict of interest was reported by the author(s).

References

[1] Khubalkar SW, Junghare AS, Aware MV, et al. Demonstrative fractional order PID controller based DC motor drive on digital platform. ISA Trans. 2018;82:79–93.

[2] Farahani G, Rahmani K. Speed control of a separately excited DC motor using new proposed fuzzy neural algorithm based on FOPID controller. J Control Autom Electr Sys. 2019;30(5):728–740.

[3] Tripathi N, Singh R, Yadav R. Analysis of speed control of DC motor – a review study. Int J Eng Res Technol (IRJET). 2015;2(8):1616–1622.

[4] Abed WNA-D. Field voltage speed control of DC motors based foraging strategy. Int J Mechatron Electr Comput Technol IJMEC. 2015;5(15):2101–2108.

[5] Hameed1 WI, Kadhim1 AS, Al-Thuwaynee AAK. Field weakening control of a separately excited DC motor using neural network optimized by social spider algorithm. 2016;8(1):1–10.

[6] Ismeal GAM, Kyslan K, Fedák V. CAD of cascade controllers for DC drives using genetic algorithm methods. Procedia Eng. 2014;96:182–189.

[7] Ayam M, Liqaa SM, Raoof TH. Speed control For separately excited Dc motor with PID controller, GA, And PSO. Int J Recent Sci Res. 2016;7(7):12673–12678.

[8] Mohamed MEA, Guo Y. Separately excited DC motor speed tracking control using adaptive neuro-fuzzy inference system based on genetic algorithm particle swarm optimization and fuzzy auto-tuning PID. In IOP conf. series: earth and environmental science, 300; 2019.

[9] Patel A, Parikh K. Speed control of DC motor using PSO tuned PI controller. IOSR J Electr Electron Eng. 2014;9(2):4–8.

[10] Chinnappan R, Logamani P, Ramasubbu R. Fixed frequency integral sliding-mode current-controlled MPPT boost converter for two-stage PV generation system. IET Circuits Devices Syst. 2019;13(6):793–805.

[11] Yazıcı I, Yaylacı EK. Discrete-time integral terminal sliding mode based maximum power point controller for the PMSG-based wind energy system. IET Power Electron. 2019;12(14):3688–3696.

[12] Bag A, Subudhi B, Ray PK. A combined reinforcement learning and sliding mode control scheme for grid integration of a PV system. CSEE J Power Energy Syst. 2019;5(4):498–506.

[13] Mirzaa AF, Linga Q, Yaqoob Javedb M, et al. Novel MPPT techniques for photovoltaic systems under uniform irradiance and partial shading. Sol Energy. 2019;184:628–648.

[14] Cheng P, Wang J, He S, et al. Observer based asynchronous fault detection for conic-type nonlinear jumping systems and its application to separately excited DC motor. IEEE Trans Circuits Syst. 2020;67(3):951–962.

[15] Bataineh KM, Hamzeh A. Efficient maximum power point tracking algorithm for PV application under rapid changing weather condition. Hindawi Publishing Corporation, ISRN Renewable Energy. 2014;18:1–13.

[16] Trovao JP, Silva MA, Antunes CH, et al. Stability enhancement of the motor drive DC input voltage of an electric vehicle using on-board hybrid energy storage systems. Appl Energy. 2017;205(51):244–259.

[17] Chauhan S, Singh B. Grid-interfaced solar PV powered electric vehicle battery system with novel adaptive digital control algorithm. IET Power Electron. 2019;12(13):3470–3478.

[18] Peng F, Wang H, Yu L. Analysis and design considerations of efficiency enhanced hierarchical battery equalizer based on bipolar CCM buck–boost units. IEEE Trans Ind Appl. 2019;55(4):4053–4063.

[19] Kumar R, Singh B. Single stage solar PV Fed brushless DC motor driven water pump. IEEE J Emerg Sel Top Power Electron. 2017;5(3):1377–1385.

[20] Kottas TL, Karlis AD, Boutalis YS. A novel control algorithm for DC motors supplied by PVs using fuzzy cognitive networks. IEEE Access. 2018;6:24866–24876.

[21] Sen A, Singh B. Peak current detection starting based position sensor less control of BLDC motor drive for PV array Fed irrigation pump. IEEE Trans Ind Appl. 2021;57(3):2569–2577.

[22] Terki A, Moussi A, Betka A, et al. An improved efficiency of fuzzy logic control of PMBLDC for PV pumping system. Appl Math Model. 2012;36(3):934–944.

[23] Murshid S, Singh B. Implementation of PMSM drive for a solar water pumping system. IEEE Trans Ind Appl. 2019;55(5):4956–4964.

[24] Mishra AK, Singh B. An efficient control scheme of self-reliant solar-powered water pumping system using a three-level DC–DC converter. IEEE J Emerg Sel Top Power Electron. 2020;8(4):3669–3681.